



Flexible thermoelectrics: from silver chalcogenides to full-inorganic devices

Journal:	<i>Energy & Environmental Science</i>
Manuscript ID	EE-COM-06-2019-001777.R2
Article Type:	Communication
Date Submitted by the Author:	17-Aug-2019
Complete List of Authors:	<p>Liang, Jiasheng; Shanghai Institute of Ceramics Chinese Academy of Sciences, Materials Chemistry and Physics Wang, Tuo; Tsinghua University, School of Materials Science and Engineering Qiu, Pengfei; shanghai institute of ceramics, Yang, Shiqi; Shanghai Institute of Ceramics Chinese Academy of Sciences Chen, Ming; Shanghai Institute of Ceramics Chinese Academy of Sciences, Chen, Hongyi; Shanghai Institute of Ceramics Chinese Academy of Sciences Song, Qingfeng; Shanghai Institute of Ceramics Chinese Academy of Sciences Zhao, Kunpeng; Shanghai Jiao Tong University, School of Materials Science and Engineering Wei, Tian-Ran; Shanghai Institute of Ceramics, Chinese Academy of Sciences, Ren, Dudi; Shanghai Institute of Ceramics, Sun, Yi-Yang; Shanghai Institute of Ceramics, Chinese Academy of Sciences, State Key Lab of High Performance Ceramics and Superfine Microstructure Shi, Xun; shanghai institute of ceramics, He, Jian; Department of Physics and Astronomy, Clemson University Chen, Lidong; Shanghai institute of Ceramics,</p>

ARTICLE

Flexible thermoelectrics: from silver chalcogenides to full-inorganic devices

Jiasheng Liang^{a,b,†}, Tuo Wang^{a,b,†}, Pengfei Qiu^a, Shiqi Yang^{a,b}, Chen Ming^a, Hongyi Chen^{a,b}, Qingfeng Song^{a,b}, Kunpeng Zhao^a, Tian-ran Wei^a, Dudi Ren^a, Yi-Yang Sun^a, Xun Shi^{a,c*}, Jian He^d, Lidong Chen^{a*}

Received 00th January 20xx,
Accepted 00th January 20xx

DOI: 10.1039/x0xx00000x

Flexible thermoelectrics is a synergy of flexible electronics and thermoelectric energy conversion. To date, state-of-the-art thermoelectrics is based on inorganic semiconductors that afford high electron mobility but lack in mechanical flexibility. By contrast, organic materials are amply flexible but low in electrical mobility and power output; the inorganic-organic hybrid design is a viable material-level option but has critical device-level issues for practical application. Here, we report high intrinsic flexibility and state-of-the-art figures of merit (up to 0.44 at 300 K and 0.63 at 450K) in Ag₂S-based inorganic materials, opening a new avenue of flexible thermoelectrics. In flexible full-inorganic devices made of such Ag₂S-based materials, high electrical mobility yielded a normalized maximum power density up to 0.08 W·m⁻¹ near room temperature under a temperature difference of 20 K, orders of magnitude higher than organic devices and organic-inorganic hybrid devices. These results promised an emerging paradigm and market of wearable thermoelectrics.

Introduction

Flexible thermoelectrics attracts intense attention in the wake of the burgeoning flexible electronics and the demand for versatile green energy harvesting. To date, the primary bottleneck is the flexibility of material of which the thermoelectric (TE) device is made. There are three major approaches, accordingly. The first approach is a hybrid design: e.g., depositing inorganic TE material in the form of thin film on a flexible organic substrate or encapsulating bulk inorganic TE material and bendable electrodes in an organic matrix to grant some device-level flexibility¹⁻¹¹. Such hybrid design is a viable material-level option but it has inherent device-level issues, such as the reliability of inorganic-organic interfacing in real-life applications. The other two approaches, by contrast, rely on the intrinsic flexibility of TE material: either developing high TE performance out of flexible organics or searching for flexibility in high TE performance inorganic semiconductors. In the second approach, the TE performance of organics such as polyaniline (PANI)¹², poly[A_x(M-ett)]_s¹³, and poly(3,4-ethylenedioxythiophene) (PEDOT)^{14, 15} were investigated. Despite good flexibility and environmental friendliness, the inherently low carrier mobility

^{12, 16, 17}, orders of magnitude lower than those of inorganic materials, severely restricts the performance of organic device^{13, 14, 18-21}. On the other hand, the state-of-the-art thermoelectric materials are inorganic, intrinsically brittle and thus cannot meet the level of bendability, foldability, and stretchability required for a flexible TE device^{14, 15, 22}. Hence, the effort in line with the third approach – searching for flexible high performance inorganic semiconductors, is scarce, not to mention fabricating a functioning flexible full-inorganic TE device.

A surprisingly high ductility was recently discovered in inorganic semiconductor Ag₂S, promising a solution to not only the aforementioned bottleneck of flexible thermoelectrics but also the overarching challenge of next-generation flexible and stretchable electronic devices²³. It is a formidable material challenge to integrate the trait of inorganic semiconductor (aka high electrical mobility) and that of organic material (aka mechanical flexibility) in one single-phased inorganic material. Being a flexible inorganic semiconductor by itself doesn't warrant a flexible inorganic TE material, as it entails scrupulous doping efforts to manage a delicate balance between the material's TE performance and its mechanical flexibility. Such a balance is the core challenge for flexible inorganic thermoelectrics. Nonetheless, the TE promise of a flexible material is still gauged by its TE figure of merit, $zT (= \alpha^2\sigma T/\kappa)$, where α , σ , κ , and T are the Seebeck coefficient, electrical conductivity, thermal conductivity, and the absolute temperature, respectively. The power factor (PF), aka the term ($\alpha^2\sigma$), governs the normalized maximum power density (cf. **Supplementary Information**) of the TE device^{24, 25}.

In this work, we report (*i*) excellent bendability and flexibility of Ag₂(S, Se), Ag₂(S, Te), and Ag₂(S, Se, Te) compounds, with high

^a State Key Laboratory of High Performance Ceramics and Superfine Microstructure, Shanghai Institute of Ceramics, Chinese Academy of Sciences, Shanghai 200050, China.

^b University of Chinese Academy of Sciences, Beijing 100049, China.

^c State Key Laboratory of Metal Matrix Composites, School of Materials Science and Engineering, Shanghai Jiao Tong University, Shanghai, 200240, China.

^d Department of Physics and Astronomy, Clemson University, Clemson, SC, 29634, USA

† These authors contributed equally to this work.

Electronic Supplementary Information (ESI) available:

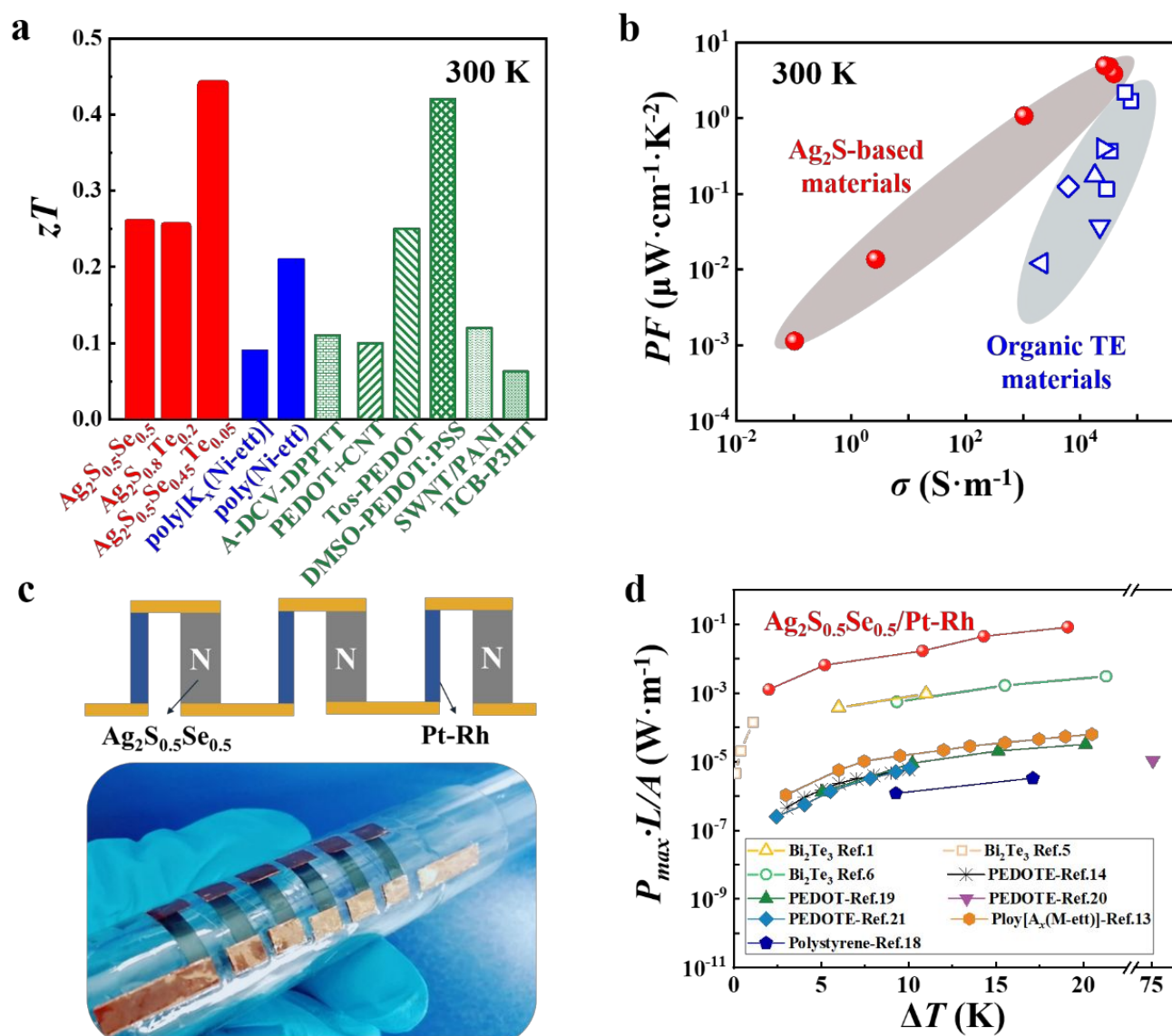


Figure 1 Ag₂S-based inorganic flexible TE materials and demonstration device. **a**) TE figure of merit zT and **b**) power factor PF for Ag₂(S, Se), Ag₂(S, Te), and Ag₂(S, Se, Te) at 300 K. Several representative organic TE materials are included for comparison. ^{12-15, 17, 26-28} **c**) Upper panel: a schematic of the Ag₂S_{0.5}Se_{0.5}/Pt-Rh in-plane device with Ag₂S_{0.5}Se_{0.5} as *n*-type legs and Pt-Ru wire as *p*-type legs. Bottom panel: optical image of a six-couple flexible Ag₂S_{0.5}Se_{0.5}/Pt-Rh TE device. The as-shown in-plane device is merely for the purpose of demonstration. A tilted architecture has been designed for better harvesting human body heat (cf. Fig. S1). **d**) Comparison of normalized maximum power density ($P_{max}L/A$) among the Ag₂(S, Se)-based inorganic TE device, inorganic-organic hybrid flexible TE devices^{1, 5, 6}, and organic flexible TE devices^{13, 14, 18-21}.

zT s up to 0.44 at 300 K and 0.63 at 450 K (cf. Fig. 1a); *(ii)* high PF s that are a few orders of magnitude higher than organic TE materials (cf. Fig. 1b) ^{12-15, 17, 26-28}, *(iii)* high normalized maximum power density up to 0.08 W·m⁻¹ for the flexible full-inorganic device made of such Ag₂S-based materials under a temperature difference of 20 K near room temperature, more than an order of magnitude higher than current inorganic-organic hybrid flexible TE devices^{1, 5, 6} and organic flexible flexible TE devices^{1, 5, 6, 13, 14, 18-21} (cf. Figs. 1c, 1d). These results promise a class of flexible inorganic TE materials towards wearable and/or curved thermoelectrics^{22, 29}.

Among silver chalcogenides Ag₂X (X=S, Se, Te), Ag₂S has poorest TE performance but excellent flexibility, whilst Ag₂Se and Ag₂Te lack mechanical flexibility but have better TE performance^{30, 31}

(cf. Fig. 2a). Here arises a key question, to what extent the Ag₂S doped by Se and Te would retain mechanically flexible and as well high TE performance? To answer, we have prepared a series of phase pure Ag₂(S, Se), Ag₂(S, Te), and Ag₂(S, Se, Te) samples (cf. **Supplementary Information** and Figs. S2). We observe that high flexibility and promising zT s coexist over a fairly broad composition range in the vicinity of room temperature (cf. Fig. 2a); notably, the level of flexibility is comparable with that of organic TE materials (cf. Fig. 2b). Figs. 2c and 2d show the room temperature mechanical properties of bulk Ag₂(S, Se) samples. Similar to Ag₂S³², the Ag₂(S, Se) samples exhibit an engineering strain above 12% without cracking in the three-point bending tests, and a maximal deformation about 50% engineering strain in the compression

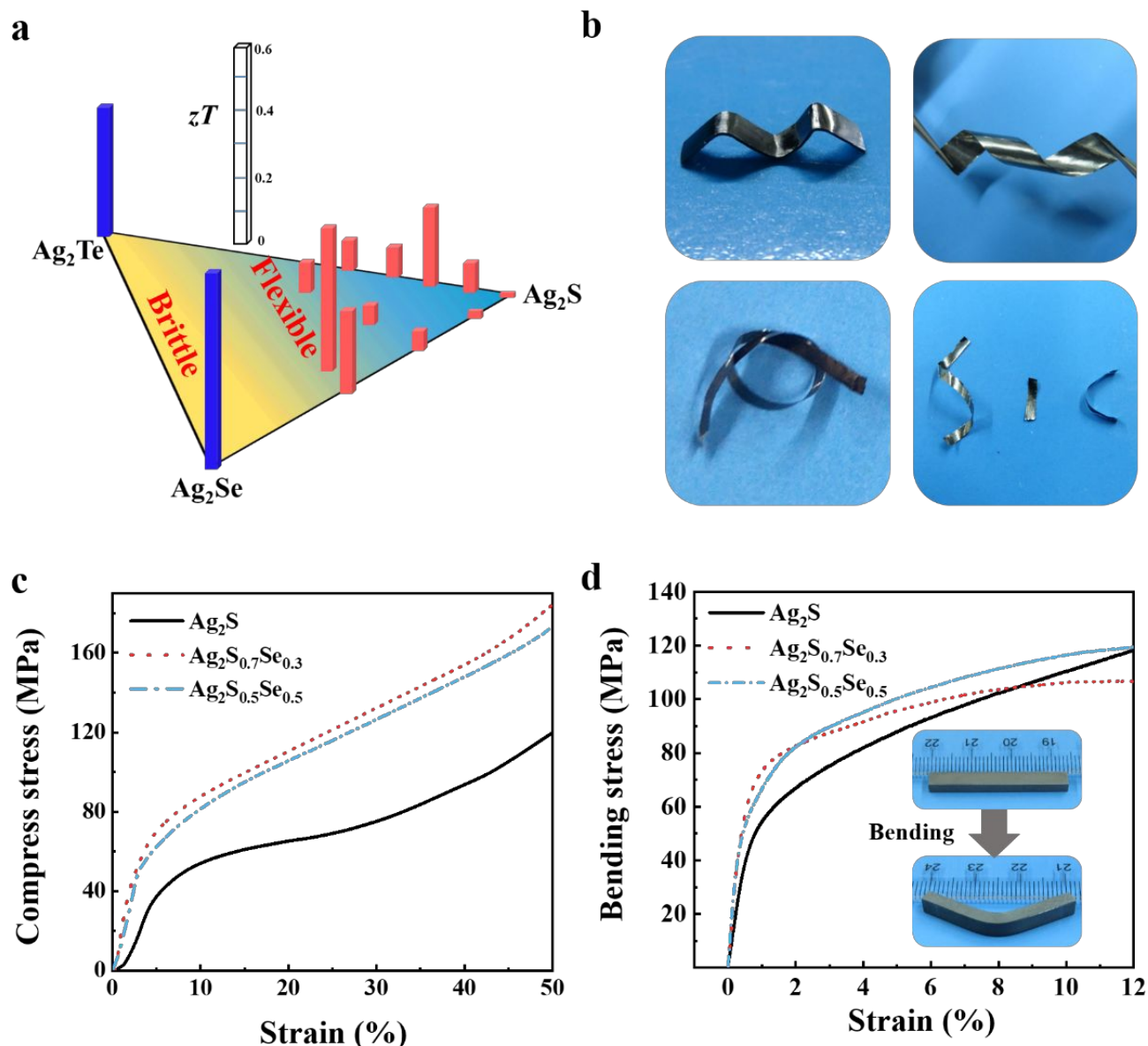


Figure 2 The flexibility- zT phase diagram and mechanical flexibility of Ag_2S -based inorganic TE materials. **a)** The flexibility- zT phase diagram of Ag_2S - Ag_2Se - Ag_2Te system. The data of Ag_2Se and Ag_2Te are taken from Refs. 30 and 31. **b)** The $\text{Ag}_2\text{S}_{0.5}\text{Se}_{0.5}$ and $\text{Ag}_2\text{S}_{0.8}\text{Te}_{0.2}$ samples twisted to various shapes. Room temperature strain-stress curves for **c)** compressing tests and **d)** bending tests of $\text{Ag}_2\text{S}_{1-x}\text{Se}_x$ ($x = 0, 0.3, \text{ and } 0.5$). The insets in **d)** show the optical images of a $\text{Ag}_2\text{S}_{0.5}\text{Se}_{0.5}$ sample before and after bending tests. The bended samples can be mechanically restored to its initial shape.

tests. The shear modulus (G_T), bulk modulus (B_T), and Poisson's ratio (ν) are important gauges of a material's mechanical properties. Empirically, the B_T/G_T ratio higher than 1.75 and ν higher than 0.26 are taken as an indicator of the ductility³³. The room temperature G_T and B_T values for $\text{Ag}_2(\text{S}, \text{Se})$ and $\text{Ag}_2(\text{S}, \text{Te})$ are calculated from the measured sound speeds (cf. Table S1 and the details in **Supplementary Information**). As shown in Table S1, all the Ag_2S -based materials studied possess B_T/G_T ratios larger than 3.9 and ν higher than 0.38 supporting their good ductility.

High flexibility and high zT s are two key ingredients of flexible thermoelectrics. On top of high flexibility, $\text{Ag}_2(\text{S}, \text{Se})$, $\text{Ag}_2(\text{S}, \text{Te})$, and $\text{Ag}_2(\text{S}, \text{Se}, \text{Te})$ exhibit good TE properties near room temperature (cf. Fig. 3). With increasing Se or Te content, the monoclinic-cubic phase transition temperature of Ag_2S is

substantially suppressed (Table S1). The electrical conductivity (σ) behavior of pristine Ag_2S is typical of an intrinsic semiconductor. The room temperature σ value of Ag_2S is as small as $0.1 \text{ S}\cdot\text{m}^{-1}$. With increasing Se or Te content, the σ increases to a value of $3.0 \times 10^4 \text{ S}\cdot\text{m}^{-1}$ for $\text{Ag}_2\text{S}_{0.5}\text{Se}_{0.5}$ and $2.7 \times 10^4 \text{ S}\cdot\text{m}^{-1}$ for $\text{Ag}_2\text{S}_{0.5}\text{Se}_{0.45}\text{Te}_{0.05}$ at 300 K, about five orders of magnitude higher than that of Ag_2S . These large σ values are comparable to those state-of-the-art brittle inorganic TE materials³⁴⁻³⁷. All $\text{Ag}_2(\text{S}, \text{Se})$, $\text{Ag}_2\text{S}_{0.8}\text{Te}_{0.2}$, and $\text{Ag}_2\text{S}_{0.5}\text{Se}_{0.45}\text{Te}_{0.05}$ possess negative Seebeck coefficient (α), indicating that electrons are the primary carrier. With increasing σ , the α gradually decreases with increasing Se or Te content in the entire temperature range studied. The α value at 300 K is $-123 \mu\text{V}\cdot\text{K}^{-1}$ for $\text{Ag}_2\text{S}_{0.5}\text{Se}_{0.5}$ and $-136 \mu\text{V}\cdot\text{K}^{-1}$ for $\text{Ag}_2\text{S}_{0.5}\text{Se}_{0.45}\text{Te}_{0.05}$, respectively, about one-tenth of Ag_2S . Nonetheless, the $|\alpha|$

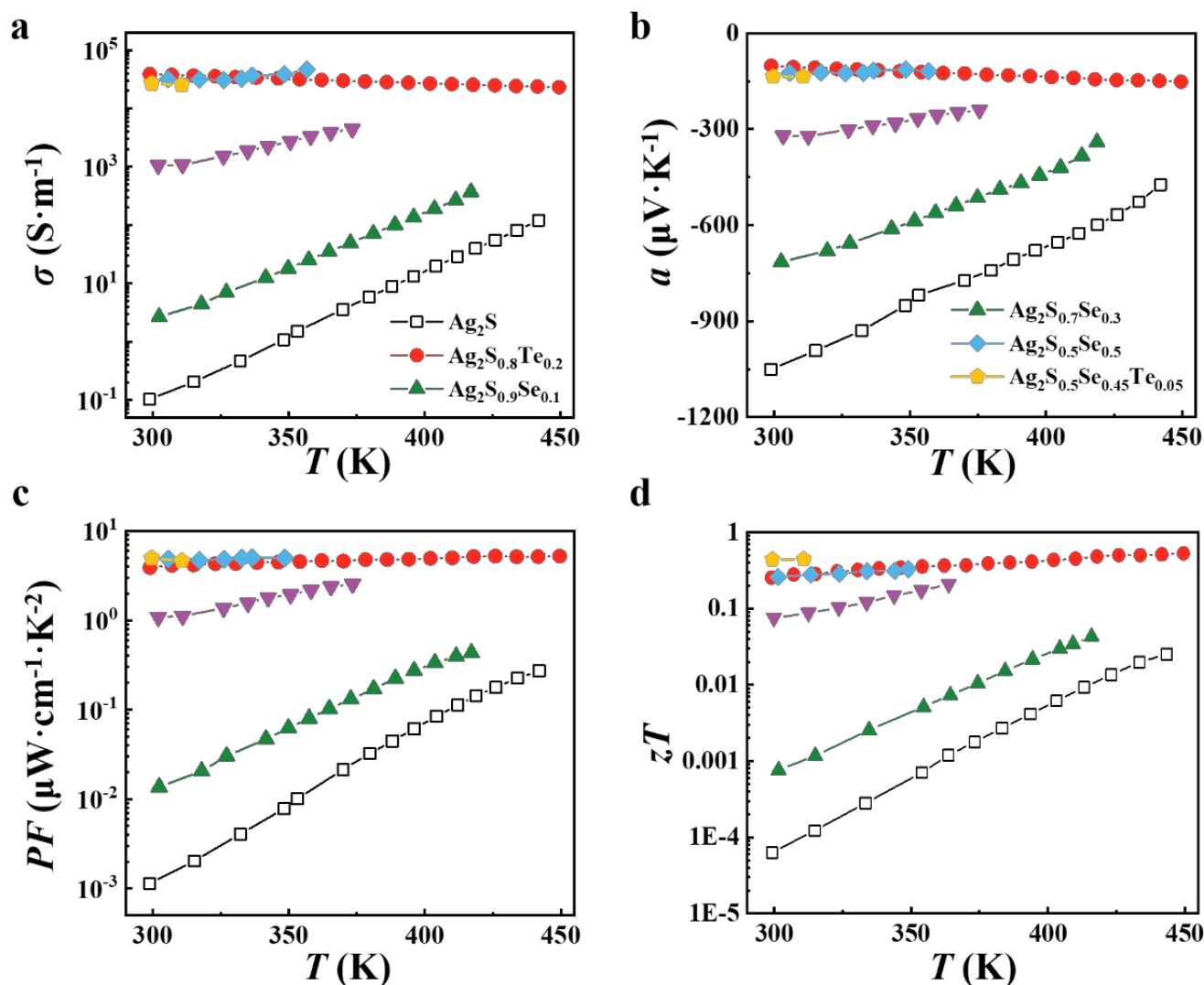


Figure 3 Thermoelectric properties of flexible Ag_2S -based inorganic TE materials. Temperature dependences of **a**) electrical conductivity σ , **b**) Seebeck coefficient α , **c**) Power factor $PF (= \alpha^2\sigma)$, and **d**) TE figure of merit zT for $\text{Ag}_2\text{S}_{1-x}\text{Se}_x$ ($x = 0, 0.1, 0.3, \text{ and } 0.5$), $\text{Ag}_2\text{S}_{0.8}\text{Te}_{0.2}$, and $\text{Ag}_2\text{S}_{0.5}\text{Se}_{0.45}\text{Te}_{0.05}$.

values are fairly large compared to organic TE materials^{12, 16, 17} that typically have an $|\alpha|$ of a few dozens of $\mu\text{V}\cdot\text{K}^{-1}$. Due to the significantly enhanced σ , the PF ($PF = \alpha^2\sigma$) is enhanced to a maximum value of $4.8 \mu\text{W}\cdot\text{cm}^{-1}\cdot\text{K}^{-2}$ for $\text{Ag}_2\text{S}_{0.5}\text{Se}_{0.5}$ and $5.0 \mu\text{W}\cdot\text{cm}^{-1}\cdot\text{K}^{-2}$ for $\text{Ag}_2\text{S}_{0.5}\text{Se}_{0.45}\text{Te}_{0.05}$ at 300 K, about four orders of magnitude higher than that for Ag_2S (Fig. 3c).

$\text{Ag}_2(\text{S}, \text{Se})$, $\text{Ag}_2(\text{S}, \text{Te})$, and $\text{Ag}_2(\text{S}, \text{Se}, \text{Te})$ have very low κ values in the range of $0.3\text{--}0.6 \text{ W}\cdot\text{m}^{-1}\cdot\text{K}^{-1}$ at 300–450 K (see Fig. S3a), among the lowest values observed in fully densified inorganic solids³⁸. The electronic thermal conductivity (κ_c) is calculated by the Wiedemann-Franz relation³⁶ $\kappa_c = L T \sigma$, where L is the Lorenz number (cf. Fig. S3b). The κ_L is obtained by subtracting κ_c from the total thermal conductivity κ (cf. Fig. S3c). Fig. S3d summarizes the κ_L for $\text{Ag}_2(\text{S}, \text{Se})$ at 300 K. For Ag_2S , the κ_L is about $0.55 \text{ W}\cdot\text{m}^{-1}\cdot\text{K}^{-1}$. Wang *et al.*³⁹ have calculated the phonon dispersion relations for Ag_2S . One eminent feature is a branch of low lying optical phonon modes located (around 3 meV). These low-frequency optical phonon modes typically interrupt the heat transport of acoustic phonons with similar frequencies,

at least partially accounting for the intrinsically low κ_L of Ag_2S . Alloying Se and/or Te at the S-site further reduces κ_L by introducing point defects to scatter heat-carrying phonons that are of short wavelengths near room temperature. Such reduction of κ_L is well accounted by the classic Callaway model⁴⁰ (cf. more details in **Supplementary Information**).

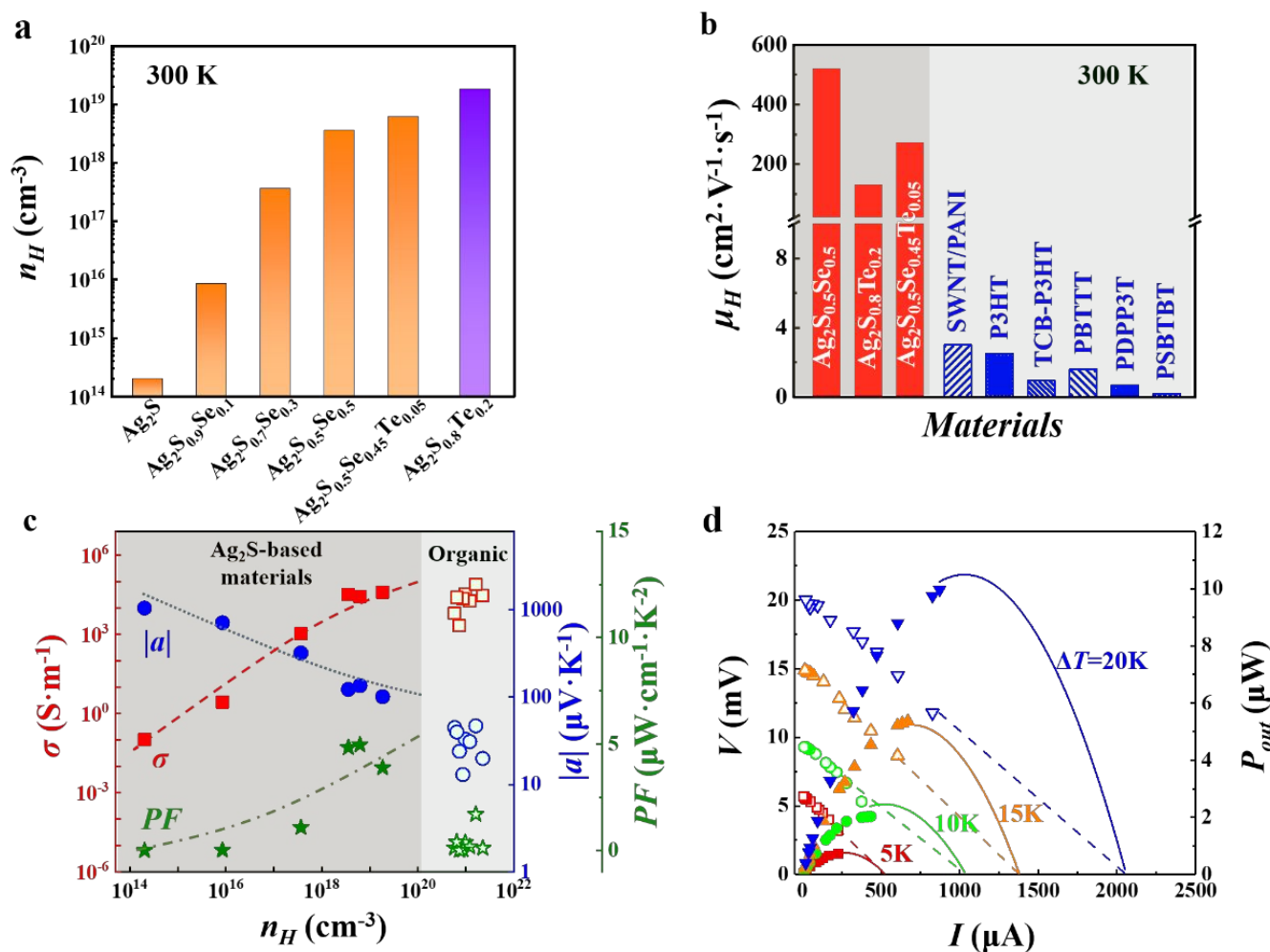


Figure 4 Room temperature electrical properties of flexible Ag_2S -based TE materials and device. **a**) Hall carrier concentration n_H for the Ag_2S (Se), $\text{Ag}_2\text{S}_{0.8}\text{Te}_{0.2}$, and $\text{Ag}_2\text{S}_{0.5}\text{Se}_{0.45}\text{Te}_{0.05}$. **b**) Comparison of carrier mobility μ_H between flexible Ag_2S -based inorganic materials and organic TE materials.^{12,16,17} **c**) Electrical conductivity σ , the absolute value of Seebeck coefficient $|\alpha|$, and power factor PF as a function of n_H . The lines are guides to the eyes. **d**) Output voltage V and power output P_{out} as a function of current (I) for a six-couple $\text{Ag}_2\text{S}_{0.5}\text{Se}_{0.5}/\text{Pt-Rh}$ device under different operating temperature difference. The cold side temperature is fixed at 293 K.

We obtained a zT value of 0.26 for $\text{Ag}_2\text{S}_{0.5}\text{Se}_{0.5}$, 0.44 for $\text{Ag}_2\text{S}_{0.5}\text{Se}_{0.45}\text{Te}_{0.05}$ at 300 K and 0.63 for $\text{Ag}_2\text{S}_{0.8}\text{Te}_{0.2}$ at 450 K (cf. Fig. 3d), which are comparable with or higher than those of organic TE materials^{12-15, 17, 26-28} (cf. Fig. 1a). More importantly, the TE properties of these flexible inorganic materials have excellent repeatability and reproducibility. For example, the variations of α and σ for the 10 μm thick $\text{Ag}_2\text{S}_{0.5}\text{Se}_{0.5}$ strip are less than 10% after 1000 bending cycles with bending angle over 120° (cf. Fig. S4). In addition, the relative resistance variation of a $\text{Ag}_2\text{S}_{0.5}\text{Se}_{0.5}$ strip is practically unchanged under different bending radii, suggesting that the strain has little influence on the TE properties (cf. Fig. S5). These results corroborate that the as prepared Ag_2S -based flexible inorganic materials are suitable for mass production with easy quality control.

Compared to Ag_2S , the significantly improved PF s and zT s in $\text{Ag}_2(\text{S}, \text{Se})$, $\text{Ag}_2(\text{S}, \text{Te})$, and $\text{Ag}_2(\text{S}, \text{Se}, \text{Te})$ are mainly ascribed to increased n_H (cf. Fig. 4a and Fig. S6). Ag_2S is a nearly intrinsic semiconductor with a very low n_H of $1.6 \times 10^{14} \text{ cm}^{-3}$ at 300 K. Increasing Se or Te content significantly increases n_H . For $\text{Ag}_2\text{S}_{0.5}\text{Se}_{0.5}$ and $\text{Ag}_2(\text{S}, \text{Se}, \text{Te})$, the n_H values are increased to the

order of 10^{18} - 10^{19} cm^{-3} at 300 K, about 4-5 orders of magnitude higher than that for Ag_2S . Ag interstitials are expected the main defects to provide charge carriers in Ag_2S -based materials. As shown in Fig. S7, the DFT calculation suggests that the defect activation energies (E_d) of Ag interstitials in both Ag_2S and $\text{Ag}_2(\text{S}, \text{Se})$ are sufficiently shallow. Thus, they can be easily ionized to donate electrons. In addition, the carrier concentration n_H from Ag interstitials is also determined by their density (N_d), which is related to the defect formation energy (E_{form}). Fig. S8c shows that the E_{form} of Ag interstitial in monoclinic Ag_2S phase is 0.91 eV. When the Se concentration is gradually increased, the E_{form} of Ag interstitial is significantly reduced, which can be attributed to the small electronegativity difference between Ag and Se as compared with that between Ag and S^{41} . The reduced E_{form} results in large density of Ag interstitials N_d , which could account for the increased carrier concentration in Se- or Te-alloyed Ag_2S shown in Fig. 4a. The flexible $\text{Ag}_2(\text{S}, \text{Se})$, $\text{Ag}_2(\text{S}, \text{Te})$, and $\text{Ag}_2(\text{S}, \text{Se}, \text{Te})$ materials possess excellent electrical properties (Fig. 1b) as compared to organic TE materials, which are mainly underpinned by their

large μ_H . In polycrystalline materials, large μ_H values often suggest light carrier effective mass (m^*)³⁸. As shown in Fig. S8d, highly dispersive bands dominated by Ag-5s electrons are found at the conduction band minimum (CBM) with a m^* of 0.27–0.47 m_0 for electrons (see Table SII), where m_0 is the mass of free electron. Such small m^* values explain the observed high μ_H values in $\text{Ag}_2(\text{S}, \text{Se})$, likewise for other Ag-based TE materials (e.g. CuAgSe ⁴² and Ag_2Se ³⁰). In the same vein, alloying Se at the S-site not only substantially reduces the band gap but also alters the shape of CBM yielding smaller m^* (cf. Fig. S8d). For example, the carrier effective mass along the $\Gamma \rightarrow Y$ direction is decreased from 0.46 m_0 for Ag_2S to 0.37 m_0 for $\text{Ag}_2\text{S}_{0.5}\text{Se}_{0.5}$ (cf. Table SII). Hence, the reduced m^* accounts for that $\text{Ag}_2\text{S}_{0.5}\text{Se}_{0.5}$ has much higher μ_H than Ag_2S (cf. Table SI). Fig. 4b summarizes the room temperature μ_H values of $\text{Ag}_2(\text{S}, \text{Se})$, $\text{Ag}_2(\text{S}, \text{Te})$, $\text{Ag}_2(\text{S}, \text{Se}, \text{Te})$, and a number of representative organic TE materials. Clearly, the μ_H values of these Ag_2S -based materials are about two or three orders of magnitude higher than those of organic TE materials. These flexible Ag_2S -based materials can achieve similar σ values of those organic TE materials but at lower carrier concentrations (Fig. 4c). A low carrier concentration generally favors a higher Seebeck coefficient. Thus, both large α and high σ can be easily achieved in $\text{Ag}_2(\text{S}, \text{Se})$, $\text{Ag}_2(\text{S}, \text{Te})$, and $\text{Ag}_2(\text{S}, \text{Se}, \text{Te})$ to realize superior PF to the organic TE materials (Figs. 1b and 4c)^{29, 43}.

Now we shift the focus from material performance to fabrication and performance of full-inorganic TE device. As the power output of a TE device is directly determined by PF of TE material^{24, 25}, the TE device based on the flexible Ag_2S -based materials displays excellent performance compared with those based on organic TE materials despite relatively high lattice thermal conductivities (Fig. S9). A six-couple in-plane TE device (Fig. 1c) consisting of n -type $\text{Ag}_2\text{S}_{0.5}\text{Se}_{0.5}$ and p -type Pt-Rh wires is fabricated with the dimension of $3 \times 15 \times 0.1 \text{ mm}^3$ for $\text{Ag}_2\text{S}_{0.5}\text{Se}_{0.5}$ legs. Copper foils are used as the electrodes to connect $\text{Ag}_2\text{S}_{0.5}\text{Se}_{0.5}$ and Pt-Rh wires. The internal electrical resistance of the as-prepared in-plane TE device is around 9 Ω . The current, output voltage, and power output are measured under different temperature gradients ($\Delta T = 2 \text{ K}, 5 \text{ K}, 10 \text{ K}, 15 \text{ K},$ and 20 K), which are shown in Fig. 4d. Due to the high α , a maximum open circuit voltage of 20 mV is obtained at $\Delta T = 20 \text{ K}$ (cf. Fig. 4d). With increasing ΔT , the maximum power output (P_{max}) is gradually increased due to the enhanced open circuit voltage and short circuit current (cf. Fig. 4d and Fig. S10a). When $\Delta T = 20 \text{ K}$, P_{max} reaches a peak value of 10 μW . This leads to a normalized maximum power density of 0.08 $\text{W}\cdot\text{m}^{-1}$ (cf. Fig. 1d), more than two orders of magnitude higher than those for current organic TE devices^{13, 14, 18–21}.

The in-plane $\text{Ag}_2(\text{S}, \text{Se})$ -based TE device can be easily and repeatedly bent in all directions. Upon > 100 bending cycles at a bending radius of 10 mm, the change of electrical resistance of the device is small (cf. Fig. S10b). Note that the in-plane design is for the purpose of *proof of concept*, it is yet optimized for harvesting human body heat. We have successfully fabricated a tilted flexible TE device out of the same $\text{Ag}_2(\text{S}, \text{Se})$ -based materials for better harvesting the body heat (cf. Fig. S1), the new architecture elevated the cold end away from skin to

increase the temperature difference. All of these results provide a testimony to the feasibility, robustness, reliability, and configurability of flexible inorganic TE generators for wearable thermoelectrics.

In summary, we report on a series of flexible inorganic Ag_2S -based TE materials with good carrier mobility, outstanding power factor, and high zT value up to 0.44 at 300 K and 0.63 at 450 K, a crucial step towards flexible thermoelectrics. A six-couple $\text{Ag}_2\text{S}_{0.5}\text{Se}_{0.5}/\text{Pt-Rh}$ in-plane TE device exhibits a high normalized maximum power density of 0.08 $\text{W}\cdot\text{m}^{-2}$, which is superior to all current flexible organic TE devices. These results greatly accelerate the development of flexible thermoelectrics towards bendable sensors and electronics.

Experimental section

Sample Synthesis. Ag_2S -based materials with the chemical formula $\text{Ag}_2\text{S}_{1-x}\text{Se}_x$ ($x = 0, 0.03, 0.1, 0.3,$ and 0.5), $\text{Ag}_2\text{S}_{0.8}\text{Te}_{0.2}$, and $\text{Ag}_2\text{S}_{0.5}\text{Se}_{0.45}\text{Te}_{0.05}$ were prepared from high purity elemental Ag (99.999%, Alfa Aesar, shots), S (99.999%, Alfa Aesar, powders), Se (99.999%, Alfa Aesar, shots), and Te (99.999%, Alfa Aesar, shots). The stoichiometric admixture was weighed out, loaded into a BN crucible, sealed in an evacuated quartz tube, heated to 1000 $^\circ\text{C}$, dwelt for 12 hours before slowly furnace-cooled to 100 $^\circ\text{C}$ within 25 hours. After that, the tube was annealed for 5 days at 450 $^\circ\text{C}$ to obtain the final product. The ingot was crashed into fine powders in stainless steel mortar filled with liquid nitrogen. Then, spark plasma sintering process was conducted at 190 $^\circ\text{C}$ for 20 min under a pressure of 50 MPa to obtain dense bulk samples for further characterization.

Sample Characterization. The phase of the samples was examined by X-ray diffraction (XRD) analysis (D8 ADVANCE instrument, Bruker Co. Ltd). Phase composition analysis was carried out by the Energy Dispersive Spectrometer (EDS, ZEISS® Supra 55). The sound speed data were obtained on an ultrasonic measurement system (RITEClab®, UMS-100) with shear wave transducers of 5 MHz and longitudinal wave transducers of 10 MHz. Electrical conductivity and Seebeck coefficient were measured using the modified thermal expansion equipment (Netzsch, DIL 402C) from 300 K up to the monoclinic-cubic phase transition temperature. The thermal conductivity was calculated from the formula $\kappa = DC_p d$, where the thermal diffusivity (D) was measured by using the laser flash method (Netzsch® LFA 457), the specific heat capacity (C_p) was measured by differential scanning calorimetric (Netzsch® DSC 404F3), and the density (d) was measured by using the Archimedes method. Hall coefficient (R_H) was measured in a Physical Property Measurement System (Quantum Design®) by sweeping the magnetic field between $\pm 3 \text{ T}$. Hall carrier concentration (n_H) and Hall mobility (μ_H) were estimated by the relations $n_H = 1/eR_H$ and $\mu_H = \sigma R_H$, respectively. Bending tests and compressing tests on the bulk specimens were conducted on an Instron® 5566 universal machine with a loading rate of 0.5 mm/min. The specimen dimension for bending test was about $3 \times 4 \times 32 \text{ mm}^3$. The specimen's dimension for compressing test

was about $5 \times 5 \times 10 \text{ mm}^3$. All specimens were cut directly from the as-prepared ingot.

Device fabrication and tests. Thin slices of $\text{Ag}_2\text{S}_{0.5}\text{Se}_{0.5}$ with a thickness of 0.1 mm were directly cut from the as-spark-plasma-sintered ingot using a diamond saw (KJ group, SYJ-160). The cutting speed is 80 rpm. The slices were cut into long strips with a width of 3 mm and a length of 15 mm by the scissors. The direction is the same as that for the TE properties measurement. The Pt-Rh wires with a diameter of 0.1 mm were used as the p-type legs. Copper foils were used as the electrodes of the device. Laser welding was used to connect copper foil and $\text{Ag}_2\text{S}_{0.5}\text{Se}_{0.5}$ strips. Silver paste was used to connect copper foil and Pt-Rh wires. A six-couple TE device was fabricated. The performance of TE device was measured using a home-built instrument with the schematic shown in Fig. S11. A series of temperature difference (2K, 5 K, 10 K, 15 K, and 20 K) was produced by heating one side of the device using a resistance heater. The temperature at two ends of the device were recorded by the K-type thermocouples pasted on the surface of the electrodes. By adjusting the resistive load in the circuit, the *I-V* curve under each temperature difference was recorded for power output calculations. Under each temperature difference, the maximum power output was reached when the resistance of external electrical load was matched with the device's internal resistance.

Code availability. Custom computer codes used in this work are available from the corresponding author upon request.

Data availability. The data supporting the findings of this study are available within the paper and its supplementary information files and available from the corresponding author upon reasonable request.

Conflicts of interest

The authors declare no competing financial interests.

Acknowledgements

Funding: This work is supported by the National Key Research and Development Program of China (2018YFB0703600), the National Natural Science Foundation of China (51625205, 51632010, 51625205, 11774365), and the Key Research Program of Chinese Academy of Sciences (KFZD-SW-421). P.Q. thanks for the support by the Youth Innovation Promotion Association of CAS under Grant No. 2016232 and Shanghai Rising-Star Program under Grant No. 19QA1410200. J. H. acknowledges the support by NSF DMR 1307740.

Author contributions

P.Q., X.S., and L.C. conceived the idea. J.L., T.W., D.R., and Q.S. performed the experimental study. S.Y. and K.Z. fabricated the device, C.M., H.C., and Y.S. performed the first-principles calculations. P.Q., T.W., X.S., J. H., and L.C. discussed and analyzed the data. J.L., P.Q., X.S., J. H., and L.C. wrote and edited the manuscript.

Additional information

Supplementary information is available in the online version of the paper. Reprints and permissions information is available online at ...Correspondence and requests for materials should be addressed to X.S., and L.C.

Notes and references

1. S. J. Kim, J. H. We and B. J. Cho, *Energy Environ. Sci.*, 2014, **7**, 1959-1965.
2. Z. Lu, M. Layani, X. Zhao, L. P. Tan, T. Sun, S. Fan, Q. Yan, S. Magdassi and H. H. Hng, *Small*, 2014, **10**, 3551-3554.
3. C. Wan, X. Gu, F. Dang, T. Itoh, Y. Wang, H. Sasaki, M. Kondo, K. Koga, K. Yabuki, G. J. Snyder, R. Yang and K. Koumoto, *Nat. Mater.*, 2015, **14**, 622-627.
4. E. S. Kim, J.-Y. Hwang, K. H. Lee, H. Ohta, Y. H. Lee and S. W. Kim, *Adv. Mater.*, 2017, **29**, 1604899.
5. F. Suarez, D. P. Parekh, C. Ladd, D. Vashae, M. D. Dickey and M. C. Ozturk, *Applied Energy*, 2017, **202**, 736-745.
6. C. S. Kim, H. M. Yang, J. Lee, G. S. Lee, H. Choi, Y. J. Kim, S. H. Lim, S. H. Cho and B. J. Cho, *Acs Energy Letters*, 2018, **3**, 501-507.
7. K. Nan, S. D. Kang, K. Li, K. J. Yu, F. Zhu, J. Wang, A. C. Dunn, C. Zhou, Z. Xie, M. T. Agne, H. Wang, H. Luan, Y. Zhang, Y. Huang, G. J. Snyder and J. A. Rogers, *Sci. Adv.*, 2018, **4**, eaau5849.
8. R. Tian, C. Wan, N. Hayashi, T. Aoi and K. Koumoto, *MRS Bull.*, 2018, **43**, 193-198.
9. L. Wang, Z. Zhang, L. Geng, T. Yuan, Y. Liu, J. Guo, L. Fang, J. Qiu and S. Wang, *Energy Environ. Sci.*, 2018, **11**, 1307-1317.
10. Q. Jin, S. Jiang, Y. Zhao, D. Wang, J. Qiu, D. M. Tang, J. Tan, D. M. Sun, P. X. Hou, X. Q. Chen, K. Tai, N. Gao, C. Liu, H. M. Cheng and X. Jiang, *Nat. Mater.*, 2019, **18**, 62-68.
11. Y. Ding, Y. Qiu, K. Cai, Q. Yao, S. Chen, L. Chen and J. He, *Nat Commun*, 2019, **10**, 841.
12. Q. Yao, Q. Wang, L. Wang and L. Chen, *Energy Environ. Sci.*, 2014, **7**, 3801-3807.
13. Y. Sun, P. Sheng, C. Di, F. Jiao, W. Xu, D. Qiu and D. Zhu, *Adv. Mater.*, 2012, **24**, 932-937.
14. O. Bubnova, Z. U. Khan, A. Malti, S. Braun, M. Fahlman, M. Berggren and X. Crispin, *Nat. Mater.*, 2011, **10**, 429-433.
15. G. H. Kim, L. Shao, K. Zhang and K. P. Pipe, *Nat. Mater.*, 2013, **12**, 719-723.
16. Q. Zhang, Y. Sun, W. Xu and D. Zhu, *Macromolecules*, 2014, **47**, 609-615.
17. S. Qu, Q. Yao, L. Wang, Z. Chen, K. Xu, H. Zeng, W. Shi, T. Zhang, C. Uher and L. Chen, *NPG Asia Mater.*, 2016, **8**, e292-e292.
18. K. Suemori, S. Hoshino and T. Kamata, *Appl. Phys. Lett.*, 2013, **103**.
19. Q. Wei, M. Mukaida, K. Kirihara, Y. Naitoh and T. Ishida, *RSC Adv.*, 2014, **4**, 28802-28806.
20. Y. Du, K. Cai, S. Chen, H. Wang, S. Z. Shen, R. Donelson and T. Lin, *Sci. Rep.*, 2015, **5**, 6411.
21. K. Zhang, J. Qiu and S. Wang, *Nanoscale*, 2016, **8**, 8033-8041.
22. Q. Zhang, Y. Sun, W. Xu and D. Zhu, *Adv. Mater.*, 2014, **26**, 6829-6851.
23. D. H. Kim and G. D. Cha, *Nat. Mater.*, 2018, **17**, 388-389.

24. H. Wu, Y. Huang, F. Xu, Y. Duan and Z. Yin, *Adv. Mater.*, 2016, **28**, 9881-9919.
25. F. Suarez, A. Nozariasbmarz, D. Vashaee and M. C. Öztürk, *Energy Environ. Sci.*, 2016, **9**, 2099-2113.
26. Y. Sun, L. Qiu, L. Tang, H. Geng, H. Wang, F. Zhang, D. Huang, W. Xu, P. Yue, Y. S. Guan, F. Jiao, Y. Sun, D. Tang, C. A. Di, Y. Yi and D. Zhu, *Adv. Mater.*, 2016, **28**, 3351-3358.
27. D. Huang, H. Yao, Y. Cui, Y. Zou, F. Zhang, C. Wang, H. Shen, W. Jin, J. Zhu, Y. Diao, W. Xu, C. A. Di and D. Zhu, *J. Am. Chem. Soc.*, 2017, **139**, 13013-13023.
28. H. Wang, S.-i. Yi, X. Pu and C. Yu, *ACS Applied Materials & Interfaces*, 2015, **7**, 9589-9597.
29. B. Russ, A. Glauddell, J. J. Urban, M. L. Chabinyk and R. A. Segalman, *Nat. Rev. Mater.*, 2016, **1**.
30. M. Ferhat and J. Nagao, *J. Appl. Phys.*, 2000, **88**, 813-816.
31. Y. Pei, N. A. Heinz and G. J. Snyder, *Journal of Materials Chemistry*, 2011, **21**.
32. X. Shi, H. Chen, F. Hao, R. Liu, T. Wang, P. Qiu, U. Burkhardt, Y. Grin and L. Chen, *Nat. Mater.*, 2018, **17**, 421-426.
33. H. Zhang, X. Sun, S. Lu, Z. Dong, X. Ding, Y. Wang and L. Vitos, *Acta Mater.*, 2018, **155**, 12-22.
34. Y. Pei, X. Shi, A. LaLonde, H. Wang, L. Chen and G. J. Snyder, *Nature*, 2011, **473**, 66-69.
35. K. Biswas, J. He, I. D. Blum, C.-I. Wu, T. P. Hogan, D. N. Seidman, V. P. Dravid and M. G. Kanatzidis, *Nature*, 2012, **489**, 414.
36. H. Liu, X. Shi, F. Xu, L. Zhang, W. Zhang, L. Chen, Q. Li, C. Uher, T. Day and G. J. Snyder, *Nat. Mater.*, 2012, **11**, 422-425.
37. S. I. Kim, K. H. Lee, H. A. Mun, H. S. Kim, S. W. Hwang, J. W. Roh, D. J. Yang, W. H. Shin, X. S. Li and Y. H. Lee, *Science*, 2015, **348**, 109-114.
38. W. G. Zeier, A. Zevalkink, Z. M. Gibbs, G. Hautier, M. G. Kanatzidis and G. J. Snyder, *Angew. Chem. Int. Ed.*, 2016, **55**, 6826-6841.
39. Wang Tuo, Chen Hong-Yi, Qiu Peng-Fei, Shi Xun and C. Li-Dong, *Acta Physica Sinica*, 2019, **68**, 90201.
40. J. Callaway, *Phys. Rev.*, 1959, **113**, 1046.
41. K. Zhao, A. B. Blichfeld, H. Chen, Q. Song, T. Zhang, C. Zhu, D. Ren, R. Hanus, P. Qiu, B. B. Iversen, F. Xu, G. J. Snyder, X. Shi and L. Chen, *Chem. Mater.*, 2017, **29**, 6367-6377.
42. S. Ishiwata, Y. Shiomi, J. Lee, M. Bahramy, T. Suzuki, M. Uchida, R. Arita, Y. Taguchi and Y. Tokura, *Nat. Mater.*, 2013, **12**, 512.
43. S. Dongmin Kang and G. Jeffrey Snyder, *Nat. Mater.*, 2017, **16**, 252-257.

Broader context

Flexible thermoelectrics enables a direct and green conversion of heat from human body or environment into electricity to power wearable electronics. It also proposes a paradigm shift in materials research as flexible thermoelectrics requires the material of which the device is made to simultaneously have inorganic semiconductor-like high thermoelectric performance and organic material-like mechanical flexibility. In this work, we tackled this dilemma, on both material level and device level, by fabricating a full-inorganic flexible thermoelectric device based on $\text{Ag}_2(\text{S}, \text{Se})$ and $\text{Ag}_2(\text{S}, \text{Te})$. Upon compositional optimization, these silver chalcogenides reached a delicate balance between high carrier mobility, power factor, figure of merit and good mechanical flexibility, underpinning a normalized maximum power density of device at least an order of magnitude higher than that of organic thermoelectric devices. These results, along with other recent advances in full-organic and organic-inorganic composite flexible thermoelectric devices, constitute a stride towards wearable or curved thermoelectrics, which greatly extends the scope of applications of thermoelectrics.